

1 **SUPPLEMENTARY MATERIALS**
2

3 Interactions between temperature and energy supply drive microbial
4 communities in hydrothermal sediment
5

6 *Running title: Temperature and energy supply drive microbial communities*

7

8 Lorenzo Lagostina¹, Søs Frandsen², Barbara J. MacGregor^{3,4}, Clemens Glombitza^{1,2},
9 Longhui Deng¹, Annika Fiskal¹, Jiaqi Li¹, Mechthild Doll⁵, Sonja Geilert⁶, Mark Schmidt⁶,
10 Florian Scholz⁶, Stefano Michele Bernasconi⁷, Bo Barker Jørgensen², Christian Hensen⁶,
11 Andreas Teske³, and Mark Alexander Lever^{1,2*}

12

13 ¹Institute of Biogeochemistry and Pollutant Dynamics, Eidgenössische Technische
14 Hochschule Zürich, 8092 Zürich, Switzerland

15 ²Center for Geomicrobiology, Department of BioScience, Aarhus University, DK-8000
16 Aarhus, Denmark

17 ³Department of Marine Sciences, University of North Carolina at Chapel Hill, Chapel Hill,
18 NC, 27599, USA

19 ⁴Department of Earth and Environmental Sciences, University of Minnesota, Minneapolis,
20 MN, 55455, USA

21 ⁵Faculty of Geosciences (FB 05), University of Bremen, 28359 Bremen, Germany

22 ⁶GEOMAR Helmholtz Centre for Ocean Research Kiel, Wischhofstraße 1-3, 24148 Kiel,
23 Germany

24 ⁷Department of Earth Sciences Eidgenössische Technische Hochschule Zürich, 8092,
25 Zürich, Switzerland

26

27 *To whom correspondence should be addressed: Mark Alexander Lever, Eidgenössische
28 Technische Hochschule Zürich, Institute of Biogeochemistry and Pollutant Dynamics,
29 Universitätsstrasse 16, CHN G50.3, 8092 Zürich, Switzerland; phone: +41 44 632 85 27;
30 email: mark.lever@usys.ethz.ch.

31

32 Supplementary Methods

33 Supplementary background on study area

34 The Guaymas basin is a young rift basin in the Gulf of California that is characterized by a
35 highly productive water column, that supports high sedimentation rates of phytoplankton-
36 derived organic matter to the seafloor, and vigorous seafloor and subseafloor hydrothermal
37 activity driven by active seafloor spreading²⁷. Tubular magmatic intrusions occur across the
38 entire basin through the 200 to 400m thick organic-rich sediment column^{15,27}. Magmatic
39 intrusions into the organic-rich sediment lead the ‘thermogenic’ breakdown of sedimentary
40 organic matter, which releases of methane, short chain organic acids (SCOAs), aliphatic
41 and aromatic hydrocarbons, including petroleum compounds, and labile protein and
42 carbohydrate-derived organic matter^{1,2,16,26,30,38,42}. In addition, the high temperatures caused
43 by magmatic intrusions result in sulfide production via the thermochemical reduction of
44 sulfate at temperatures >110°C¹⁹. In certain regions, vertically advecting fluids transport
45 these compounds to shallow sediments with temperatures in the growth range of microbial
46 life, where they sustain vast populations of chemoorgano- and chemolithoautotrophic
47 microorganisms, including dense mats of sulfur-oxidizing bacteria (*Beggiatoaceae*)^{31,35,41}.
48 These microorganisms in turn form the basis of a rich food web that supports a high biomass
49 of macrofauna^{20,39}. Vertical fluid advection also leads to formation of hard structures at the
50 seafloor, including hydrothermal vent chimneys and carbonate crusts^{12,47}.

51 The abundant supplies of diverse energy substrates combined with high diversity of
52 sedimentary habitats⁴⁷, and the extreme spatial and temporal variability in temperature^{31,32}
53 results in a dynamic sedimentary environment that supports functionally, physiologically,
54 and phylogenetically very diverse microbial communities^{14,24,44}. Decades of microbiological
55 cultivation have led to the isolation of many thermophilic and hyperthermophilic
56 microorganisms from hydrothermal vents and hydrothermal seep sediments^{5,6,8,22,40,45} and
57 the discovery of new catabolic pathways^{13,23}, and have expanded the known growth
58 temperature ranges of microorganisms^{18,19,22}. Many of the thermo- and hyperthermophiles
59 isolated occur in both hydrothermal seep sediments and nearby hydrothermal vent
60 chimneys^{9,24}, frequently even in samples that also harbor microorganisms with much lower
61 temperature requirements^{11,24}. Guaymas Basin sediment has also remained a treasure
62 trove of novel microbial diversity. Gene sequences of the alpha subunit of methyl coenzyme
63 M reductase (*mcrA*) indicate the presence of at least three novel candidate orders of

methane-cycling Archaea^{4,24}. Recent genomic investigations have resulted in the proposal of 5 new candidate phyla within the Bacteria and Archaea¹⁴. *In situ* fluid geochemistry and temperature, and microbial resilience to rapidly fluctuating thermal regimes, have been proposed as key drivers of microbial community structure^{12,32,34,46}. In addition, it has been proposed that high rates of thermal disturbance result in refugia for temperature-resilient microorganisms that are competitively excluded in more stable environments²⁴. The existence of such refugia, combined with the fact that Guaymas Basin sediment unites characteristics of hydrothermal vents, oil reservoirs, and hydrocarbon seeps may further contribute to the astounding microbial diversity²⁴.

Despite the impressive number of past microbiological investigations, many questions concerning the controls on microbial community structure in Guaymas Basin sediment remain open. For instance, only few studies have investigated *in situ* microbial abundances, or their relationships with temperature^{10,34}. Recent metagenomic data from 11 samples indicate that Archaea dominate hydrothermal sites¹⁴, providing support to the hypothesis that Archaea are better equipped for life at high temperatures than Bacteria because of higher temperature resistance of archaeal ether-based lipid membranes compared to bacterial ester-based lipid membranes⁴⁸.

Most microbiological research on Guaymas Basin has so far focused on a hydrothermal field with hydrothermal vents in the Southern Trough (here referred to as Seep Area (SA)). Subseafloor fluid circulation through the surrounding sediment leads to the development of a hot, heterogeneous methane, sulfide, and petroleum seep area, characterized by the presence of *Beggiatoaceae* mats, hydrothermal mounds, and bare sediments⁴⁷. Additional research has been performed on cold methane and CO₂ seeps at the northeastern transform margin (Sonora Margin)^{9,37,49}. In 2015, a second hydrothermal vent field (here referred to as Non-Seep Area (NSA)) was discovered on the flank of the Northern Trough during Expedition SO241 of the research vessel SONNE². Near this vent field, extensive authigenic carbonate crusts are present in the absence of clear fluid flow, indicating a previously active hydrothermal and cold seep environment, in which deep fluid and thermogenic gas flow terminated 7-28,000 kyrs ago¹⁶. Even though present-day vertical fluid advection was not detected at locations sampled during SO241, sites surrounding the vent field maintain significant temperature gradients, reaching temperatures of 60-70°C within 400-500 centimeters below the seafloor (mbsf)^{2,16}. Due to the absence of new energy inputs from photosynthetically produced OM or hydrothermal fluid advection, these geothermally heated

97 non-seep sites offer the opportunity to investigate the role of temperature in driving microbial
98 community structure under diffusion-controlled subseafloor conditions, where
99 microorganisms are severely energy-limited.

100 **Supplementary Methods**

101 *DNA extraction*

102 DNA was extracted according to Lever *et al.* (2015) (reference 25). Briefly, all samples were
103 extracted using lysis protocol II with the following specifications: 0.2 g sediment were placed
104 into screw-cap microcentrifuge tubes filled to ~15% with 0.1mm zirconium-silica beads and
105 mixed with 100 μ L of 10mM sodium hexametaphosphate solution. Samples were
106 homogenized for 30s at 30 shakings per second on a Tissue Lyzer LT (Qiagen). Afterward,
107 chemical lysis for 1 hour at 50°C and 600 rpm was performed on a ThermoMixer
108 (Eppendorf). Samples were then washed two times with ice-cold chloroform-isoamylalcohol
109 (24:1), and precipitated at room temperature in the dark with ethanol-sodium chloride
110 solution supplemented with linear polyacrylamide (LPA) as a co-precipitant (20 μ g LPA mL⁻¹
111 extract). Precipitated and dried DNA pellets were purified using the CleanAll DNA/RNA
112 Clean-Up and Concentration Micro Kit (Norgen Biotek, Madison, WI) according to the
113 manufacturer's instructions. For further details on Lysis Protocol II, including all instrument
114 settings, see Lever *et al.* (2015).

115 *16S rRNA gene quantification*

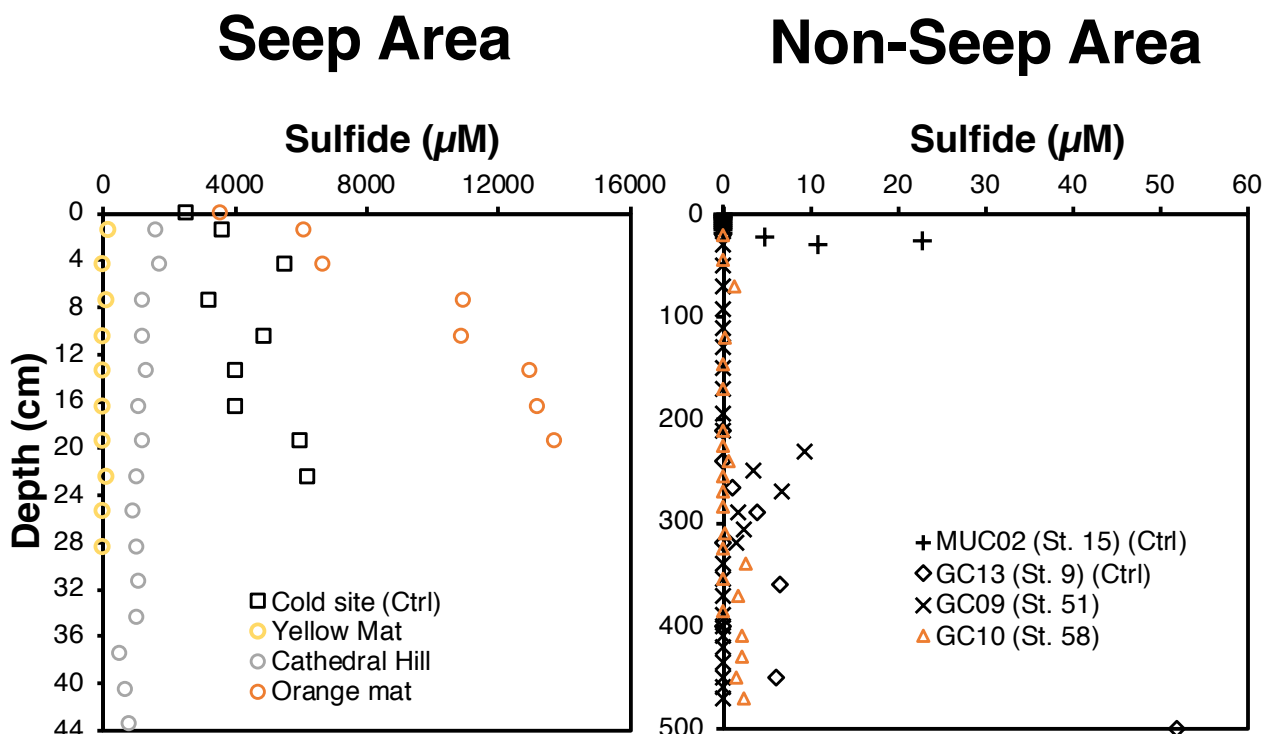
116 Bacterial and archaeal 16S rRNA gene copy numbers were quantified by SYBR-Green-
117 based quantitative PCR (qPCR) on a LightCycler 480 Instrument II (Roche Life Science,
118 Penzberg, Germany). The Bac908F_mod (5'- AAC TCA AAK GAA TTG ACG GG-3')²⁵ /
119 Bac1075R (5'- CAC GAG CTG ACG ACA RCC-3')³⁶ primer combination was used for
120 Bacteria. The Arch915F_mod (5'-AAT TGG CGG GGG AGC AC-3')⁷ / Arch1059R (5'-GCC
121 ATG CAC CWC CTC T-3')⁵¹ was used for Archaea. qPCR reactions (final volume: 10 μ L)
122 consisted of 5 μ L 2 \times SYBR Green I Master (Roche Life Science, Penzberg, Germany), 1
123 μ g μ L⁻¹ bovine serum albumin, 10 μ M of each primer, molecular-grade water, and 2 μ L of
124 original DNA extract. Amplicons of 16S rRNA genes of *Holophaga foetida* and
125 *Thermoplasma acidophilum* were used as bacterial and archaeal qPCR standards. Pure
126 cultures of *H. foetida* and *T. acidophilum* were purchased from the German Collection of
127 Microorganisms and Cell Cultures and their DNA extracted using a MOBIO PowerSoil DNA

128 Isolation Kit (QIAGEN, Hilden, Germany). Thermal cycler protocols consisted of (1) enzyme
129 activation and initial denaturation at 95 °C for 5 min; (2) 40 cycles (Bacteria) and 50 cycles
130 (Archaea) of (a) denaturation at 95°C for 10 s, (b) annealing at 60°C (Bacteria) and 55°C
131 (Archaea) for 30 s, (c) elongation at 72°C for 15 s, and (d) fluorescence measurement at
132 72°C (Bacteria) and 81°C (Archaea) for 15 s; and (3) a stepwise melting curve from 95°C to
133 55°C in 1 min to check for primer specificity. All measurements were run in duplicate.
134 Samples with on average >3 times higher values than extraction blanks were included in
135 the manuscript.

136 *16S rRNA amplicon sequencing and phylogenetic classifications*

137 According to 16S rRNA gene abundances, samples were pooled in different groups for a
138 first booster PCR, performed with the aim of increasing and normalizing the gene copy
139 number. The archaeal primer pair S-D-Arch-0519-a-A-19 (5'-C AGC MGC CGC GGT AAH
140 ACC-3'; reference 43, renamed in reference 21) / Arch915RRmod (5'-GT GCT CCC CCG
141 CCA ATT-3')⁷ and the bacterial primer pair S-D-Bact-0341-b-S-17 (5'-CCT ACG GGN GGC
142 WGC AG-3') / S-D-Bact-0785-a-A-21 (5'-GAC TAC HVG GGT ATC TAA TCC-3'; both
143 reference 17, renamed in reference 21) were used for this booster PCR. Booster PCRs were
144 used to elevate gene copy numbers to similar concentrations across samples and to
145 minimize PCR cycle numbers with tailed primers, which introduce additional biases beyond
146 those of non-tailed primers³. According to the original 16S gene copy numbers determined
147 by qPCR, booster PCR cycle numbers varied from 10 to 32. PCR products of booster PCR
148 were checked on an agarose gel, and those samples with visible (preferably weakly visible)
149 correctly-sized bands were used for downstream work. Booster PCRs were repeated on
150 samples with no visible bands, increasing the cycle number by 4 additional cycles. 1µL of
151 PCR product from all successful booster PCRs was used as template for a second PCR (8
152 cycles) with frameshifted tailed primers, that were used to improve sequencing accuracy²⁹.
153 Tailed amplicons were then cleaned using AMPure XP beads, amplicon lengths checked by
154 gel electrophoresis to confirm successful addition of adaptor (tail) sequences, and then
155 underwent Index-PCR using the Nextera DNA library Prep Kit (Illumina, San Diego, USA).
156 Indexed amplicons were cleaned using AMPure XP beads, quantified with a Tecan plate
157 reader and Tapestation (Agilent, Santa Clara, USA), and finally pooled equimolarly. Paired-
158 end sequencing (2x300 bp) was performed on a MiSeq Personal Sequencer (Illumina, San
159 Diego, USA). Raw-read ends were trimmed and pairs merged into amplicons. Subsequently
160 primers were trimmed and amplicons were quality filtered (PRINSEQ). Operational

161 taxonomic units (OTU) at 97% clustering were assigned using UNOISE. Taxonomic
162 assignments were performed using the SILVA database (SSURef v128) for Bacteria and
163 a manually curated in-house archaeal 16S rRNA gene database in ARB²⁸. Sequencing data
164 were analyzed using Phyloseq package³³. Statistical analyses were perfomed in R using
165 Vegan, heatmaps using package Corrplot⁵⁰.

166 **Supplementary Figures**

167

168 **Supplementary Figure 1.** Hydrogen sulfide concentration profiles in the Seep Area (SA)
169 and Non-Seep Area (NSA) replotted from Reference 47 (SA) and Reference 16 (NSA; also
170 see Supplementary Data 1). Note: no data exist for Everest Mound and MUC12.

171

172

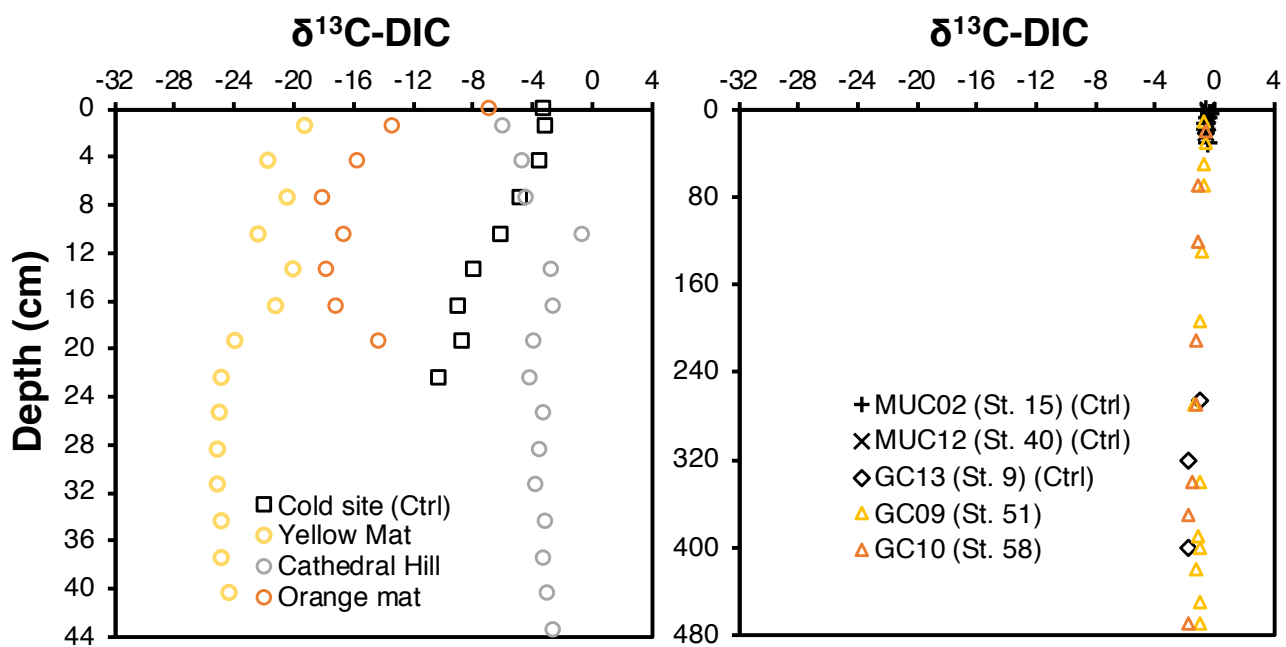
173

174

175

Seep Area

Non-Seep Area



176

177

178 **Supplementary Figure 2.** Depth profiles $\delta^{13}\text{C}$ -dissolved inorganic carbon ($\delta^{13}\text{C}$ -DIC) in the
179 Seep Area (SA) and Non-Seep Area (NSA). All data shown in Supplementary Data 1.
180

181

182

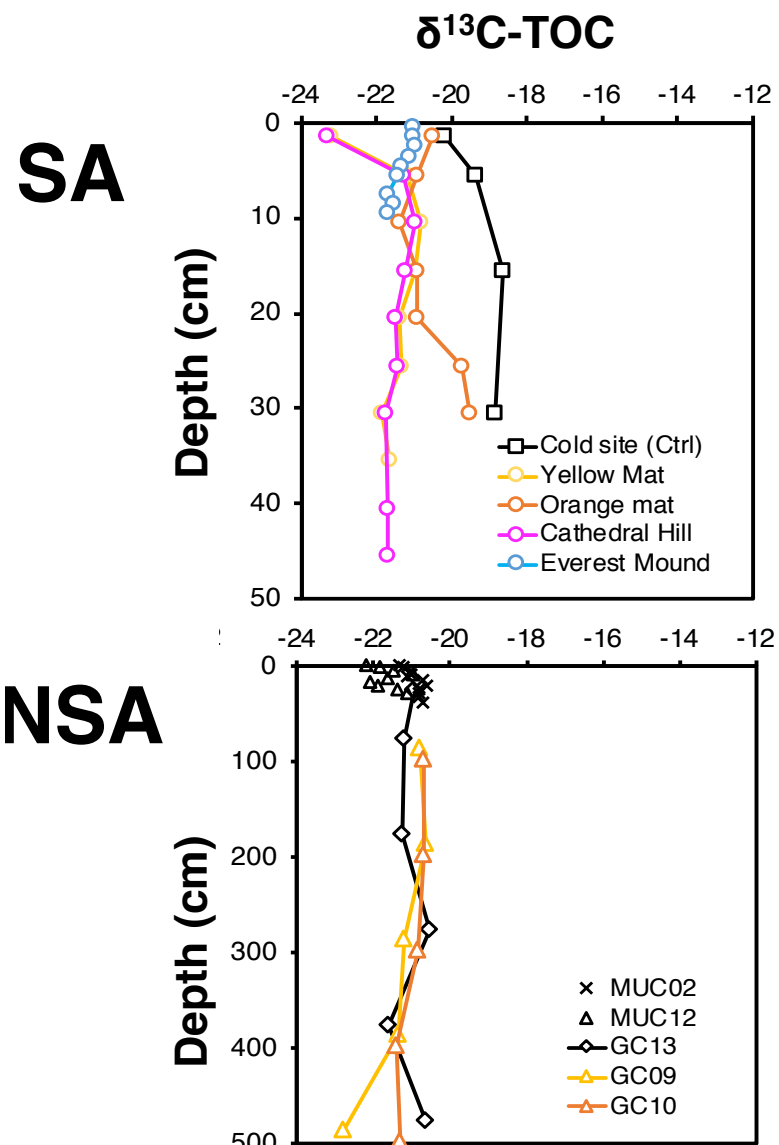
183

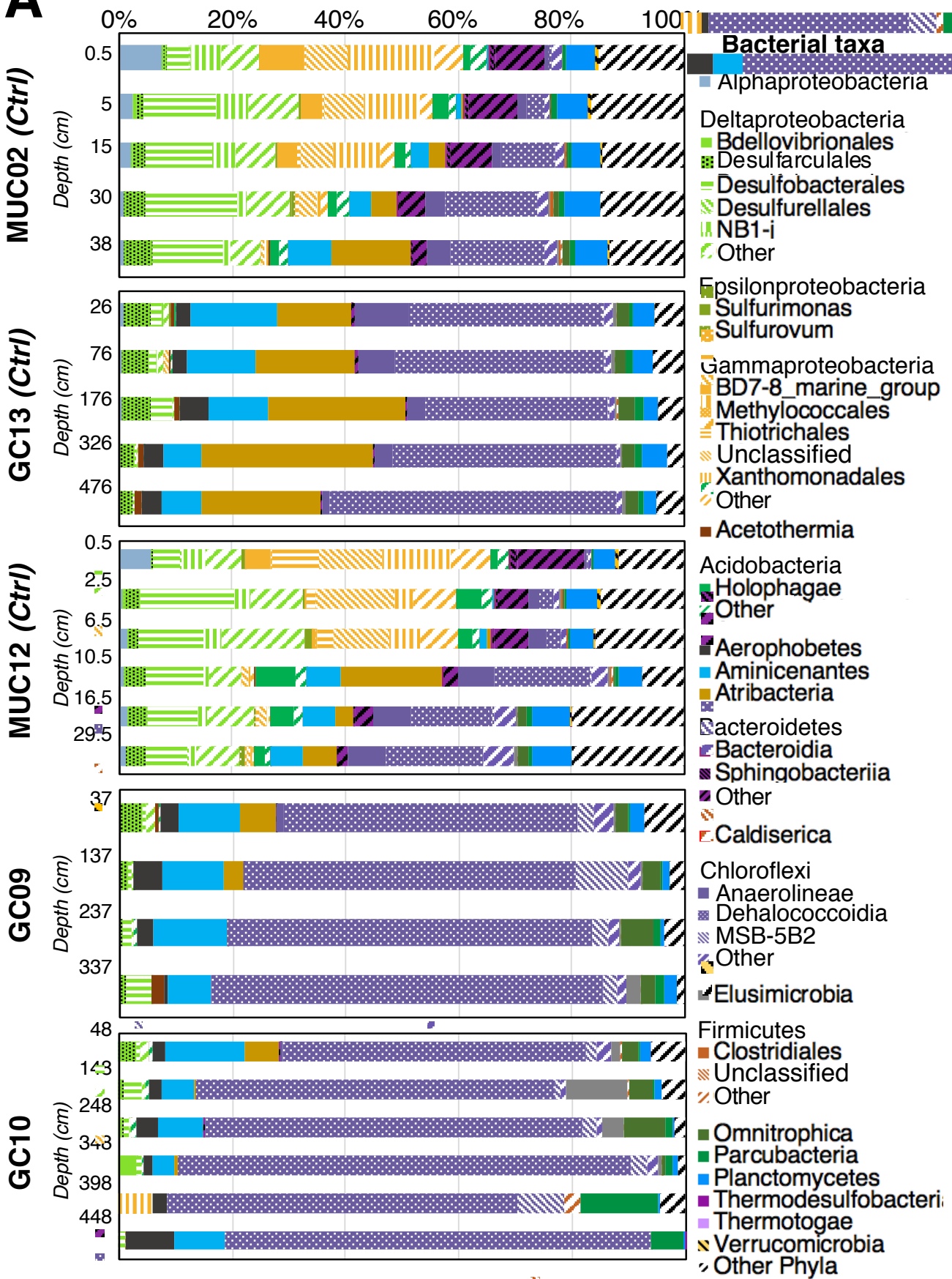
184

185

186

187

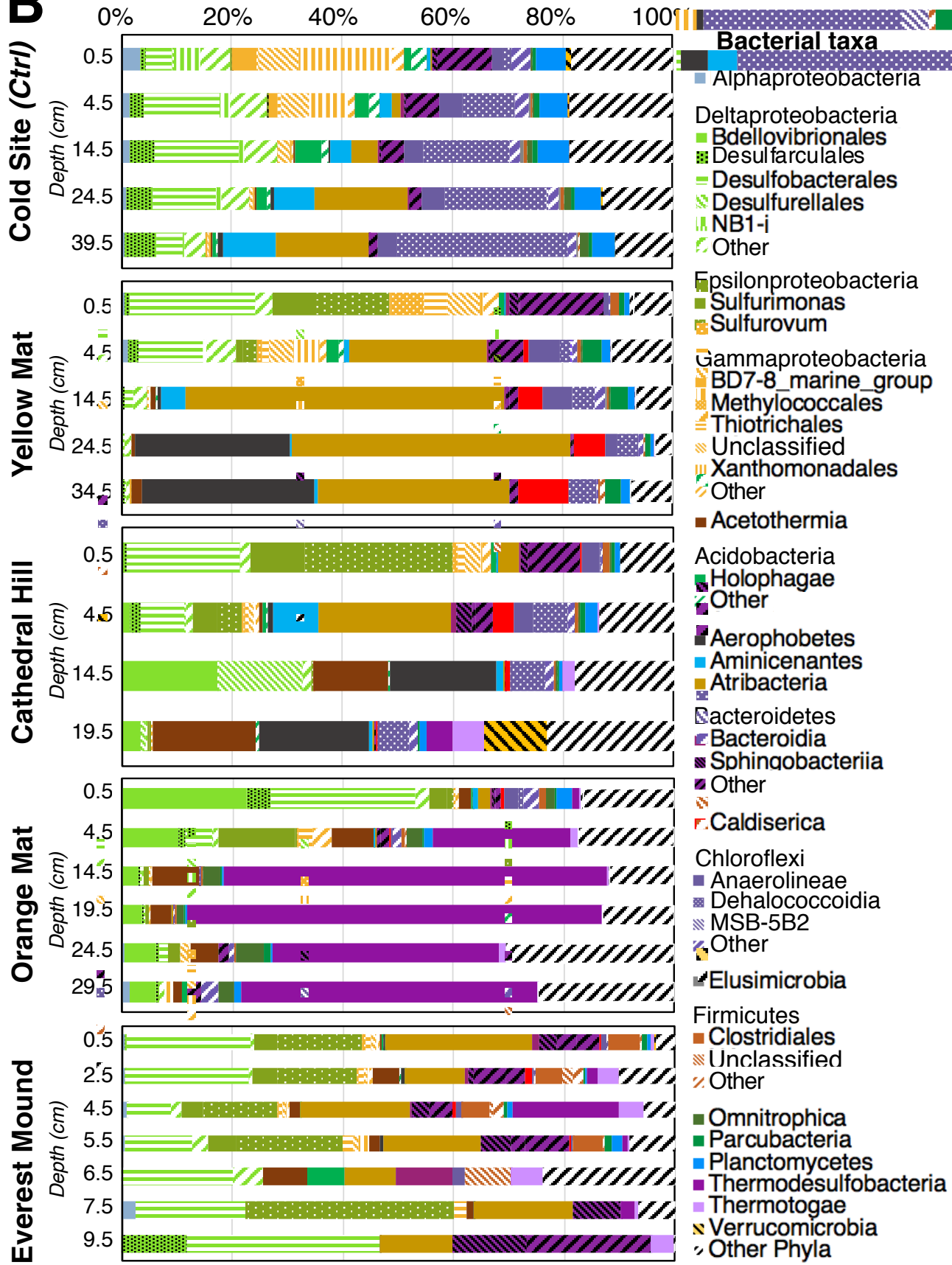


A

202

Supplementary Figure S4B, Seep Area (SA)

203

B

204

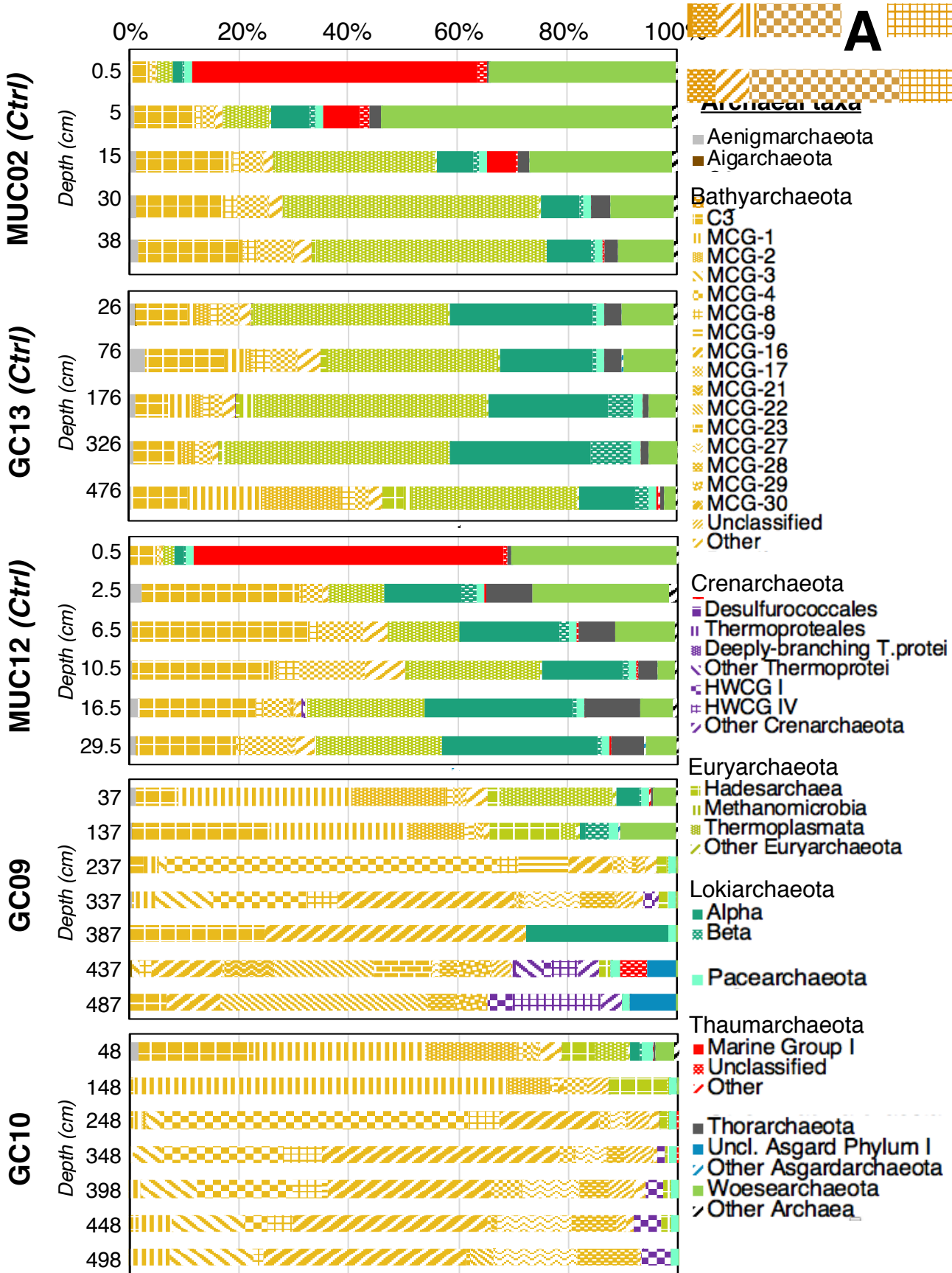
Supplementary Figure 4. Detailed depth profiles of bacterial community structure in the (a) NSA and (b) SA, focusing on the dominant classes, orders, and genera for phyla with sub-phylum classifications.

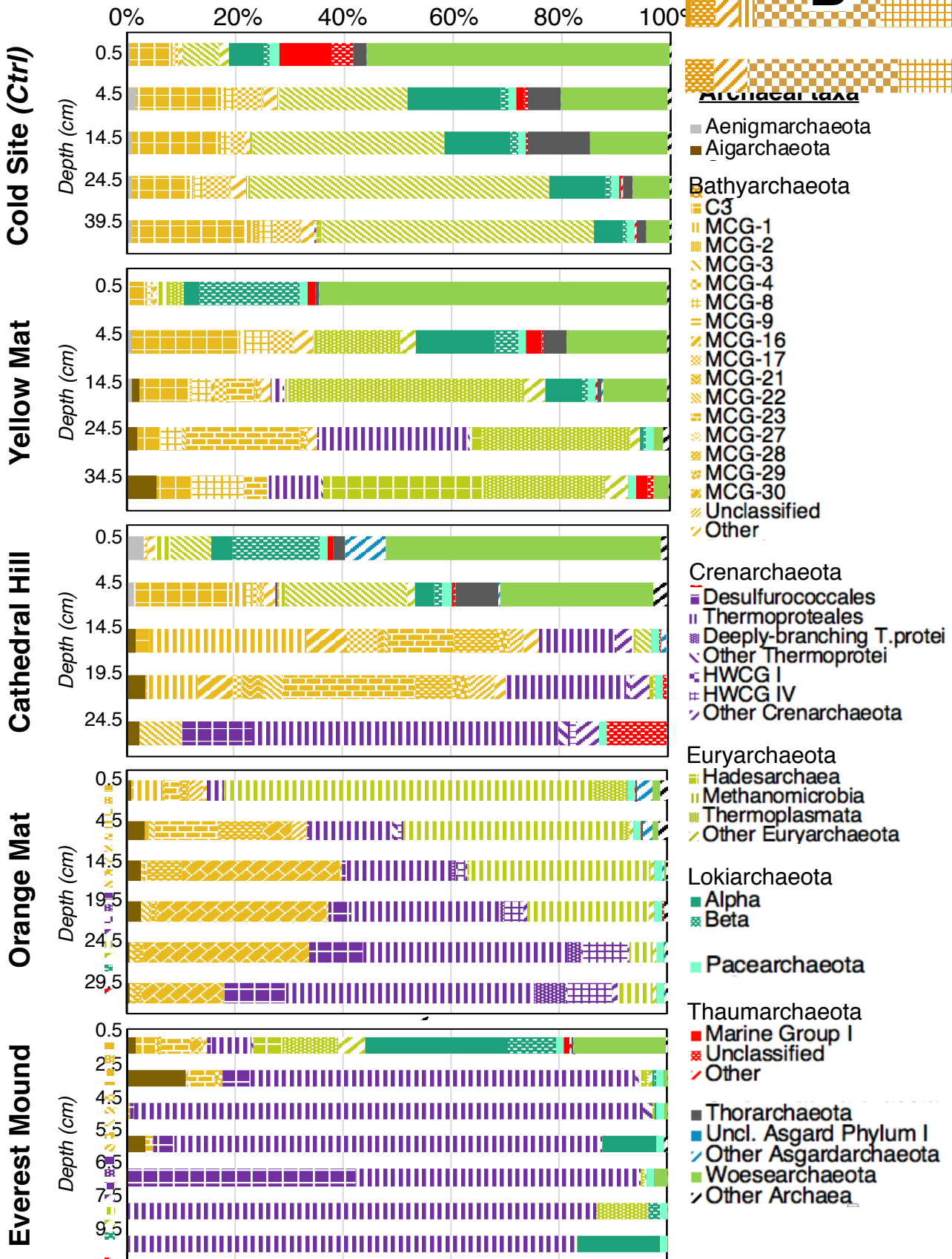
205

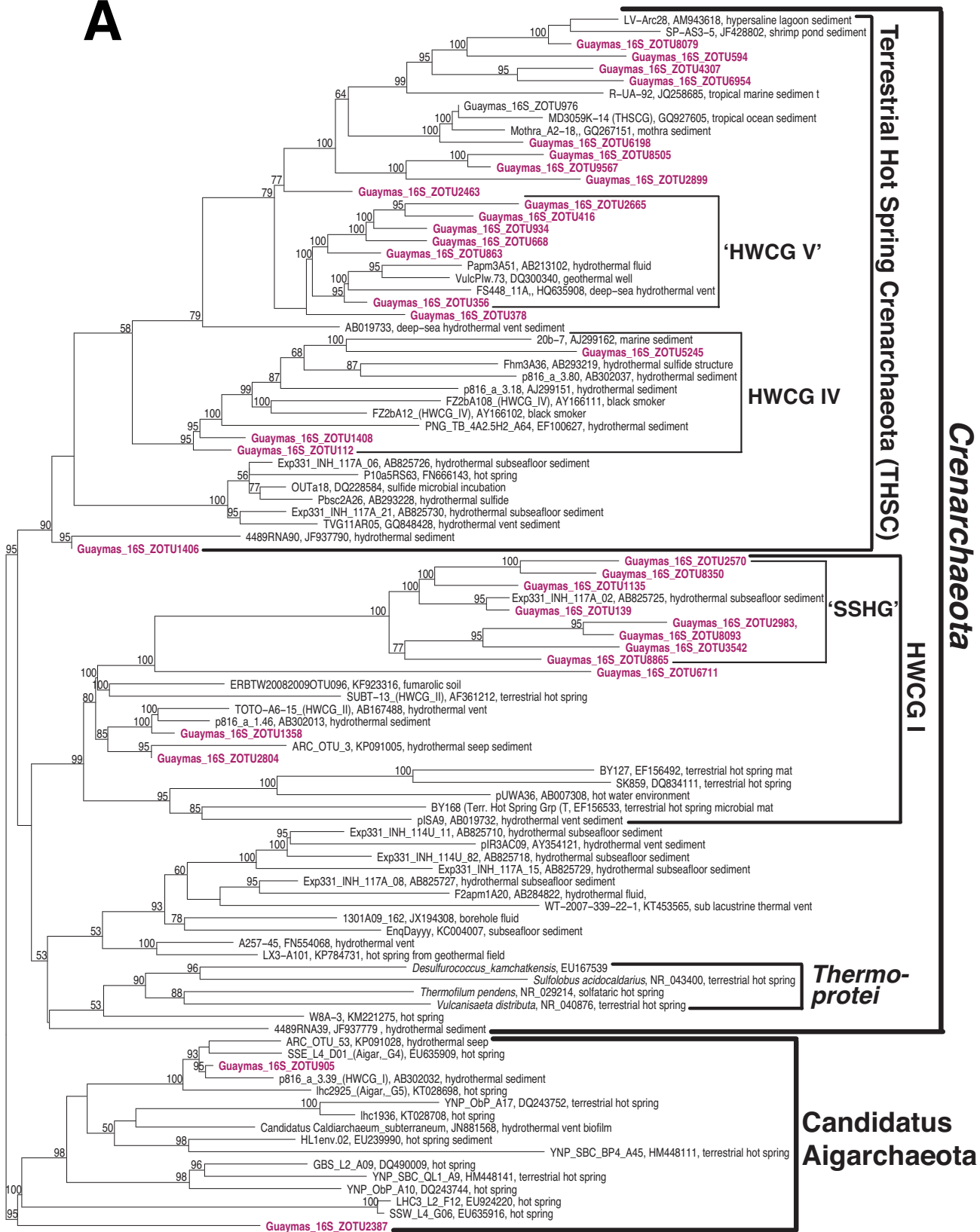
206

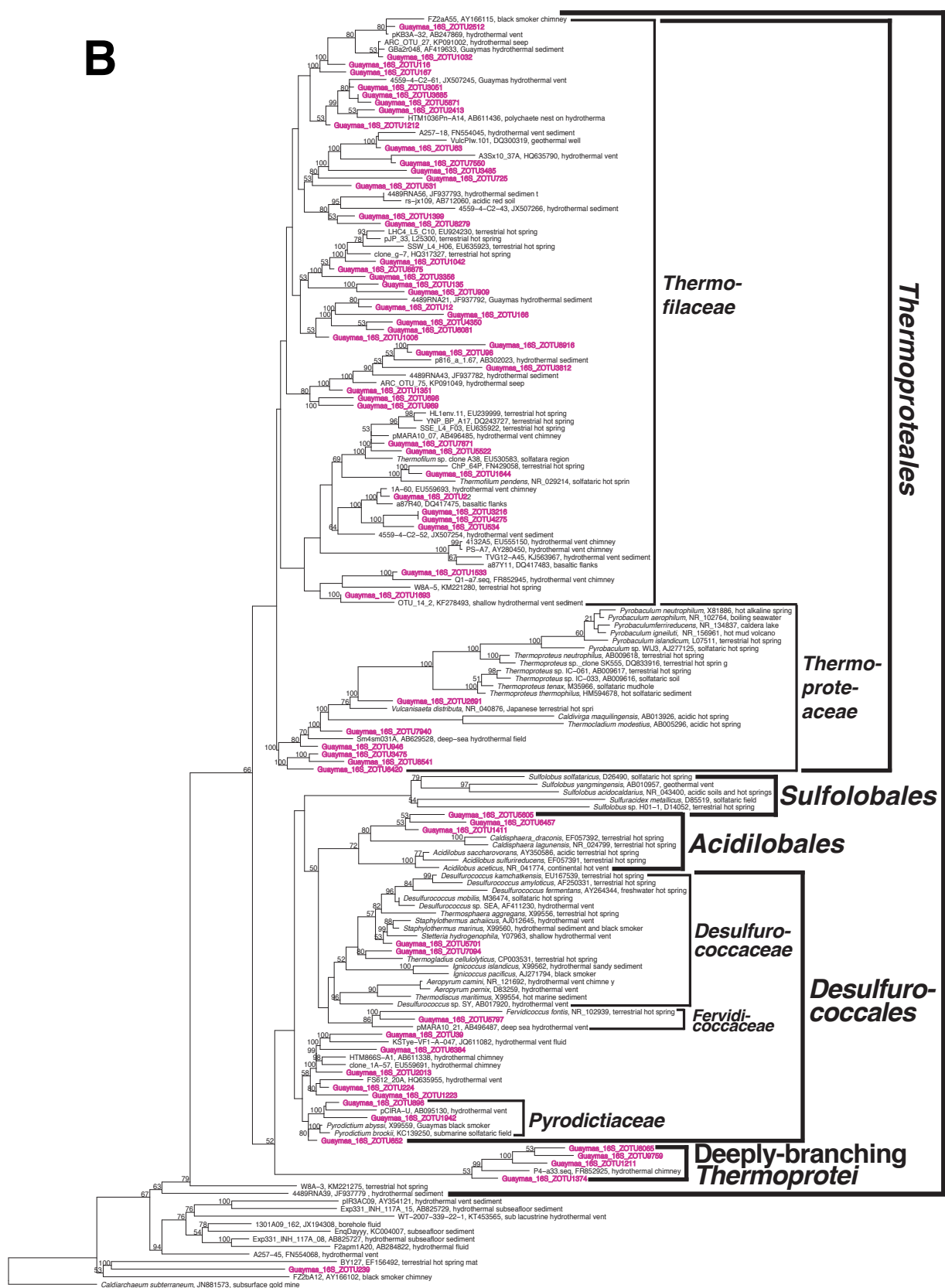
207

208



B

A

B

226 ***Previous 2 pages***

227 **Supplementary Figure 6.** Phylogenetic trees of (a) Terrestrial Hot Spring Crenarchaeota
228 (THSC) and Hot Water Crenarchaeote Group I (HWCG I) and *Aigarchaeota*, and (b) the
229 crenarchaeotal class *Thermoprotei*. Trees are based on a manually optimized archaeal 16S
230 rRNA gene alignment and were constructed by ARB Neighbor-Joining using Jukes-Cantor
231 Correction combined with a column filter that excluded insertions and hypervariable regions.
232 Subsurface Hydrothermal Group (SSHG) and Deeply-Branching *Thermoprotei* are newly
233 classified groups within the HWCG I and *Thermoprotei*, respectively. Bootstrap values
234 (1,000 repetitions) of $\geq 50\%$ are shown at branch nodes.

235

236

237

238

239

240

241

242

243

244

245

246

247

248

249

250

251

252

253

254

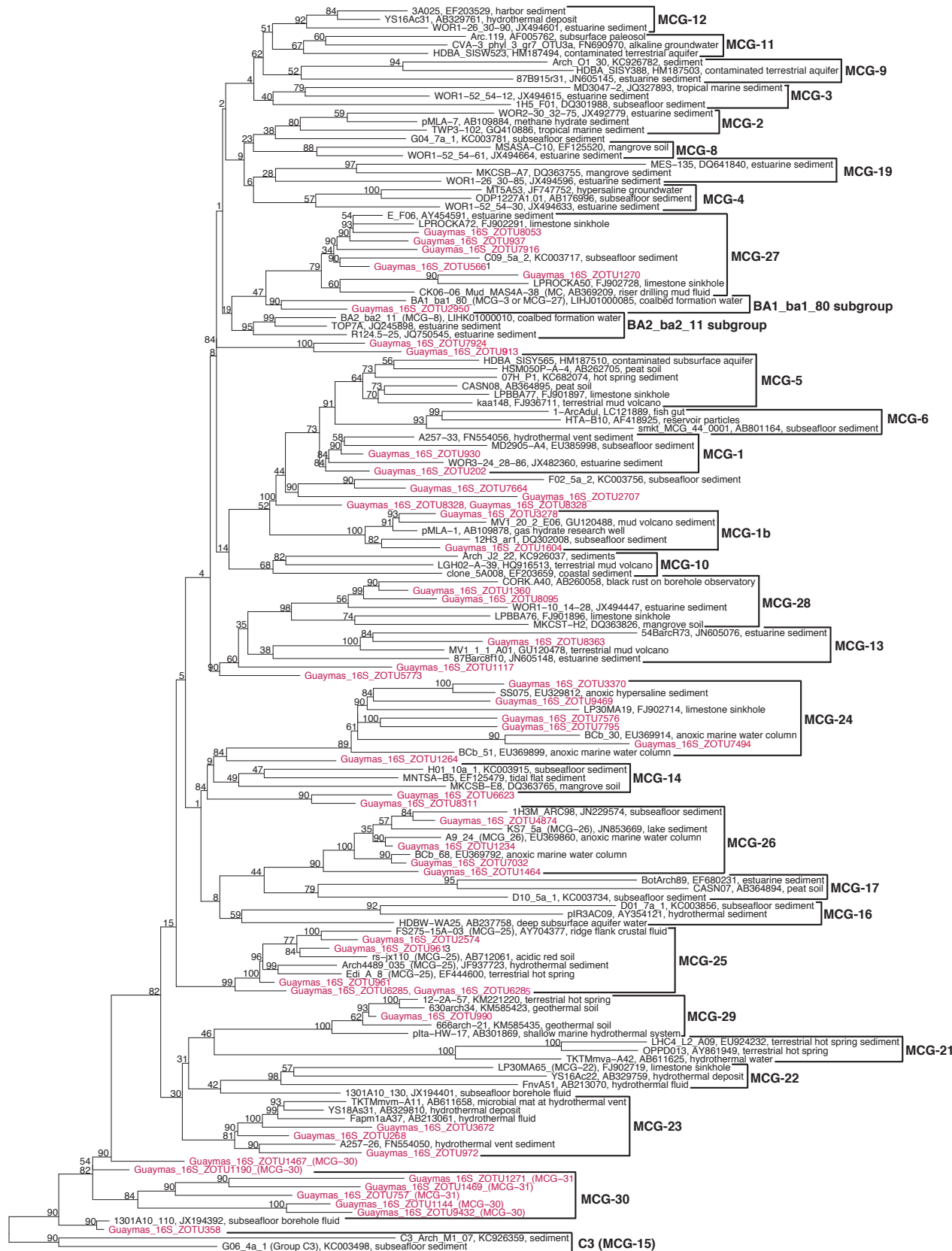
255

256

257

258

259



260

261

262

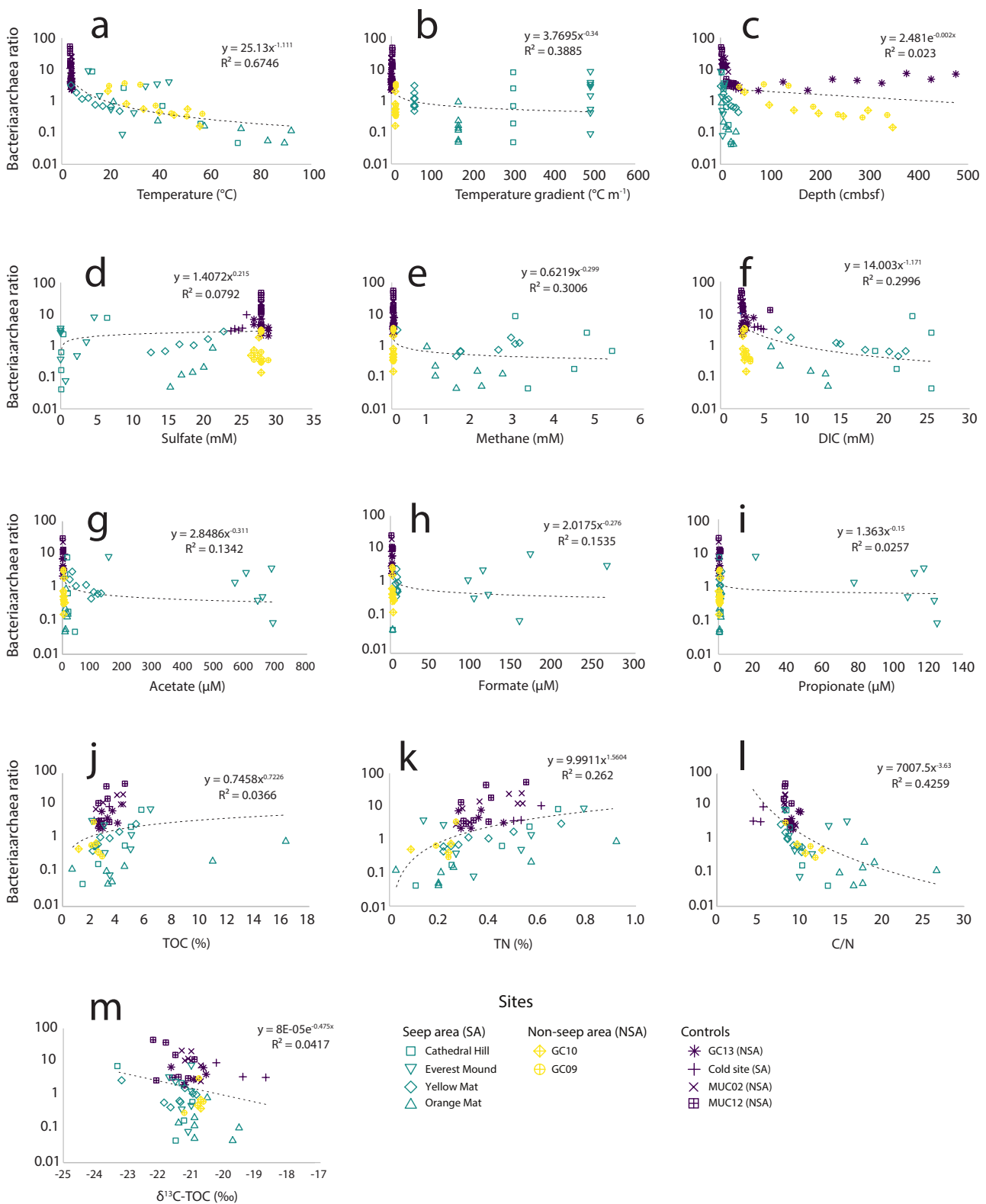
263

264

265

266

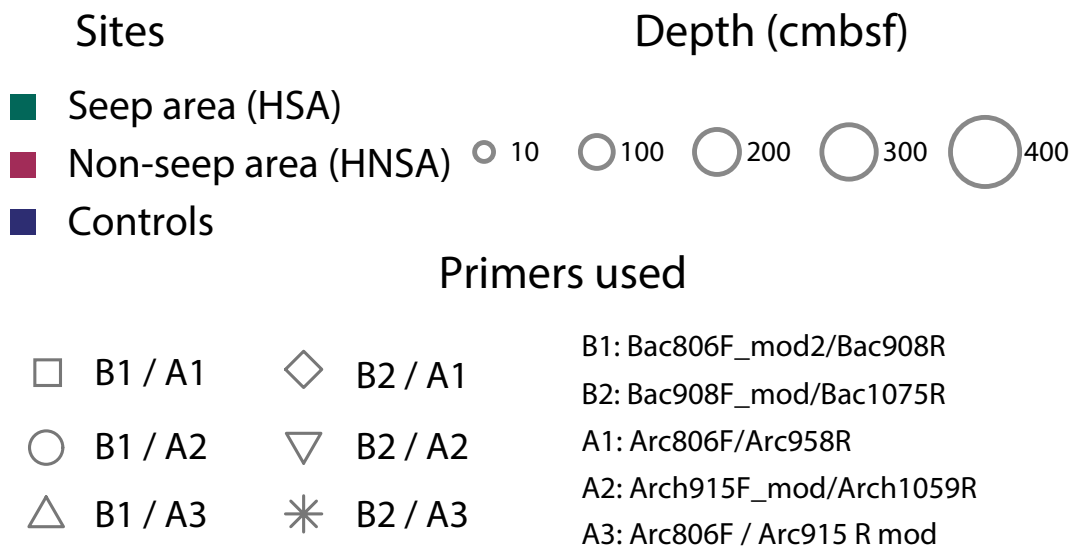
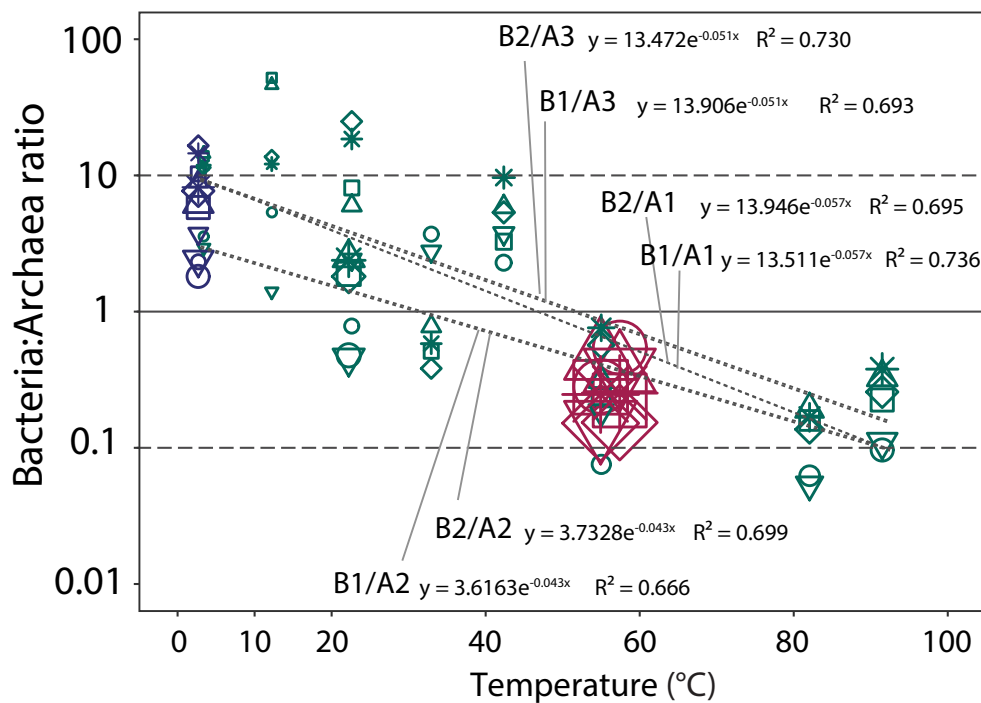
Supplementary Figure 7. Phylogenetic tree highlighting novel *Bathyarchaeota* subgroups (MCG-24 through -30), along with their closest relatives. The tree was produced by ARB Neighbor-Joining using Jukes-Cantor Correction and is based on a manually optimized archaeal 16S rRNA gene alignment with a column filter to exclude insertions and hypervariable regions. Note: C3 are also known as MCG-15. Bootstrap values (1,000 repetitions) of $\geq 50\%$ are indicated at branch nodes.



267

268

269 **Supplementary Figure 8.** Relationships between BARs and environmental variables.
 270 Environmental variables include (a) temperature, (b) temperature gradient, and (c) sediment
 271 depth, concentrations of (d) sulfate, (e) methane, (f) dissolved inorganic carbon (DIC), (g)
 272 acetate, (h) formate, and (i) propionate, as well as (j) total organic carbon (TOC), (k) total
 273 nitrogen (TN), (l) TOC/TN (C/N), and (m) δ¹³C-TOC. Trendlines reflect best-fit functions in
 274 Microsoft Excel, which was also used to calculate coefficient of determination (R^2) values.



275

276

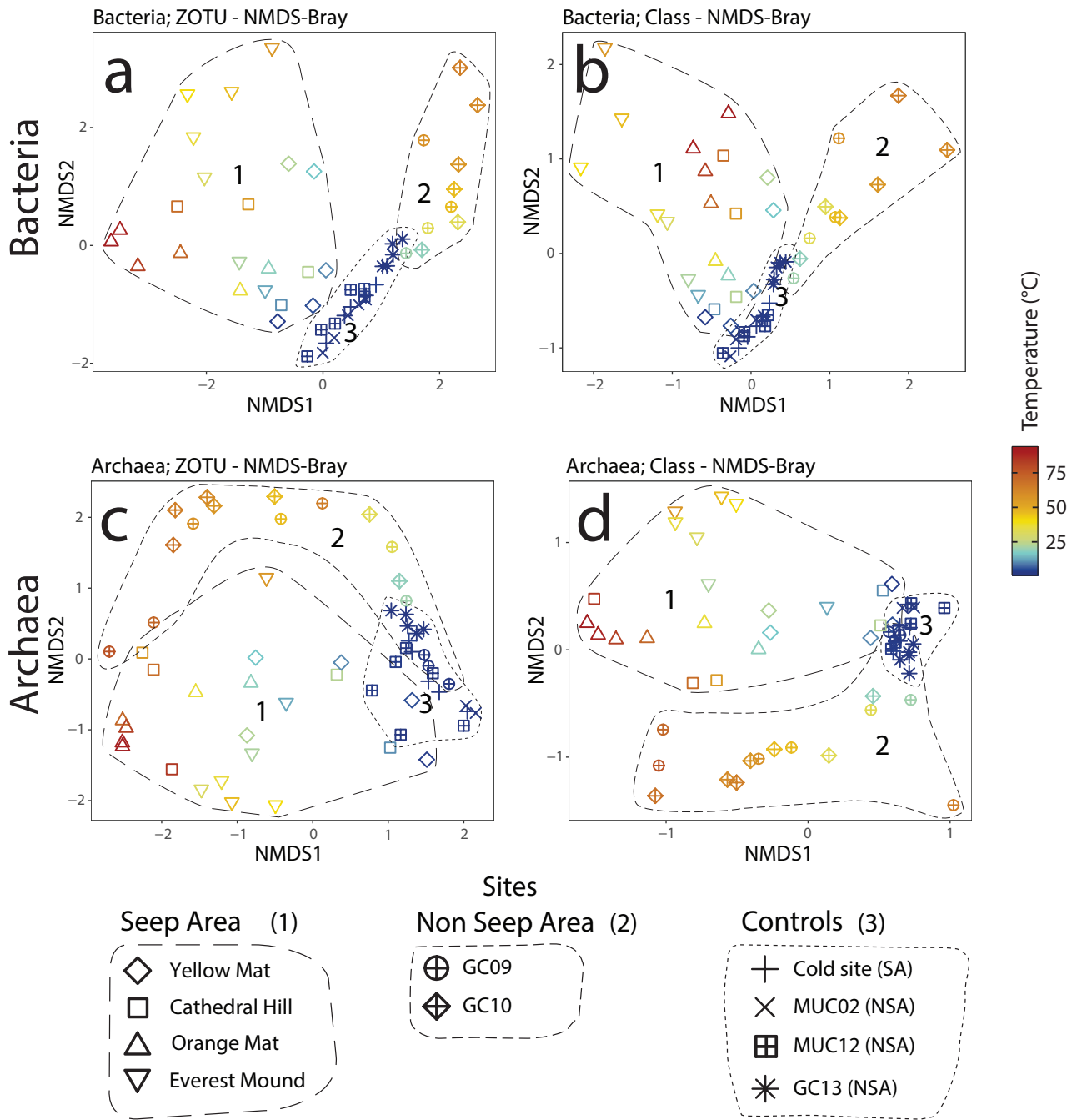
277

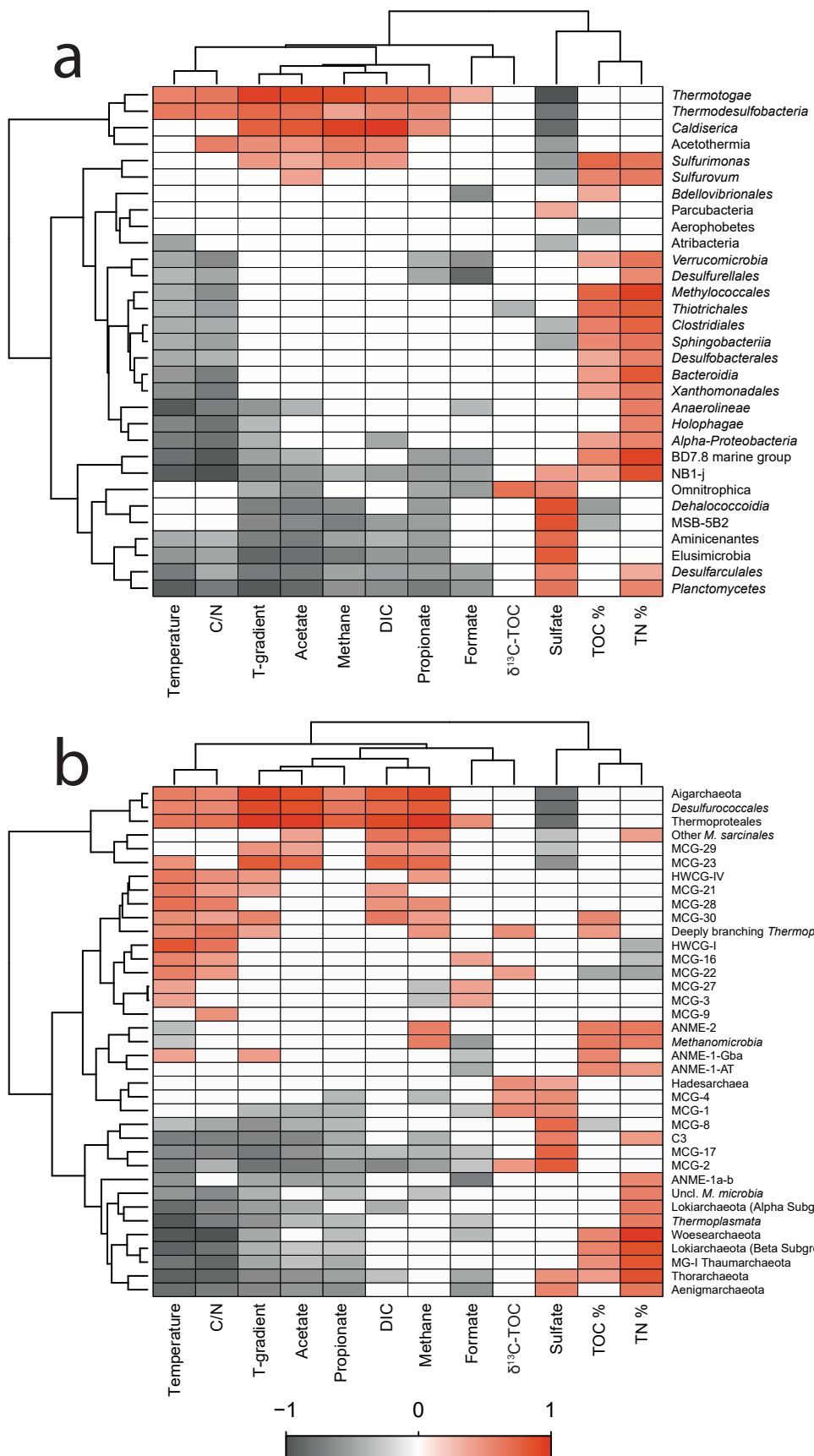
278 **Supplementary Figure 9.** Bacteria-to-Archaea 16S rRNA gene copy ratios (BARs) vs.
 279 temperature. Calculated for different bacterial and archaeal qPCR primer combinations on
 280 a subset of samples. The best-fit trendline in all cases follows an exponential function that
 281 was fitted in Microsoft Excel, which was also used to calculate the coefficient of
 282 determination (R^2) values. Results obtained with the primer pairs B2 and A2 on all samples
 283 are shown in Figures 1 and 2 and in Supplementary Figure S9.

284

285

286





298

299 **Supplementary Figure 11.** Heat map showing correlations between relative abundances
 300 of key bacterial and archaeal groups and geochemical variables based on Spearman's rank
 301 correlation coefficients. Only significant ($p < 0.05$) correlations are colored.

302 **Supplementary References**

- 303 (1) Bazylinski DA, Farrington JW, Jannasch HW. Hydrocarbons in surface sediments from
304 a Guaymas Basin hydrothermal vent site. *Org Geochem* 1988; **12**: 547-558.
- 305 (2) Berndt C, Hensen C, Mortera-Gutierrez C, Sarkar S, Geilert S, Schmidt M, *et al.* Rifting
306 under steam—How rift magmatism triggers methane venting from sedimentary
307 basins. *Geology* 2016; **44**: 767-770.
- 308 (3) Berry D, Ben Mahfoudh K, Wagner M, Loy A. Barcoded primers used in multiplex
309 amplicon pyrosequencing bias amplification. *Appl Environ Microbiol* 2011; **77**: 7846-
310 7849.
- 311 (4) Biddle JF, Cardman Z, Mendlovitz H, Albert DB, Lloyd KG, Boetius A, *et al.* Anaerobic
312 oxidation of methane at different temperature regimes in Guaymas Basin
313 hydrothermal sediments. *ISME J* 2012; **6**: 1018-1031.
- 314 (5) Burggraf S, Fricke H, Neuner A, Kristjansson J, Rouvier P, Mandelco L, *et al.*
315 *Methanococcus igneus* sp. nov., a novel hyperthermophilic methanogen from a
316 shallow submarine hydrothermal system. *Syst Appl Microbiol* 1990; **13**: 263-269.
- 317 (6) Burggraf S, Jannasch HW, Nicolaus B, Stetter KO. *Archaeoglobus profundus* sp. nov.
318 represents a new species within the sulfate-reducing Archaeabacteria. *Syst Appl*
319 *Microbiol* 1990; **13**: 24-28.
- 320 (7) Cadillo-Quiroz H, Brauer S, Yashiro E, Sun C, Yavitt J, Zinder S. Vertical profiles of
321 methanogenesis and methanogens in two contrasting acidic peatlands in central New
322 York State, USA. *Environm Microbiol* 2006; **8**: 1428-1440.
- 323 (8) Canganella F, Jones WJ, Gambacorta A, Antranikian G. *Thermococcus guaymasensis*
324 sp. nov. and *Thermococcus aggregans* sp. nov., two novel thermophilic archaea
325 isolated from the Guaymas Basin hydrothermal vent site. *Int J Syst Bacteriol* 1998;
326 **48**: 1181-1185.
- 327 (9) Cruaud P, Vigneron A, Pignet P, Caprais J-C, Lesongeur F, Toffin L, *et al.* Comparative
328 study of Guaymas Basin microbiomes: cold seeps vs. hydrothermal vents sediments.
329 *Frontiers Mar Sci* 2017; **4**: 417.
- 330 (10) Deng LH, Fiskal A, Han XG, Dubois N, Bernasconi SM, Lever MA. Improving the
331 accuracy of flow cytometric quantification of microbial populations in sediments:
332 importance of cell staining procedures. *Frontiers Microbiol* 2019; **10**: 720.

- 333 (11) Dhillon A, Lever M, Lloyd KG, Albert DB, Sogin ML, Teske A. Methanogen diversity
334 evidenced by molecular characterization of methyl coenzyme M reductase A (*mcrA*)
335 genes in hydrothermal sediments of the Guaymas Basin. *Appl Environ Microbiol*
336 2005; **71**: 4592-4601.
- 337 (12) Dick GJ. The microbiomes of deep-sea hydrothermal vents: distributed globally, shaped
338 locally. *Nature Rev Microbiol* 2019; **17**: 271-283.
- 339 (13) Dombrowski N, Seitz KW, Teske AP, Baker BJ. Genomic insights into potential
340 interdependencies in microbial hydrocarbon and nutrient cycling in hydrothermal
341 sediments. *Microbiome* 2017; **5**: 106.
- 342 (14) Dombrowski N, Teske AP, Baker BJ. Expansive microbial metabolic versatility and
343 biodiversity in dynamic Guaymas Basin hydrothermal sediments. *Nature Comm*
344 2018; **9**: 4999.
- 345 (15) Einsele G, Gieskes JM, Curray J, Moore DM, Aguayo E, Aubry MP, *et al*. Intrusion of
346 basaltic sills into highly porous sediments, and resulting hydrothermal activity. *Nature*
347 1980; **283**: 441-445.
- 348 (16) Geilert S, Hensen C, Schmidt M, Liebetrau V, Scholz F, Doll M, *et al*. On the formation
349 of hydrothermal vents and cold seeps in the Guaymas Basin, Gulf of California.
350 *Biogeosciences* 2018; **15**: 5715-5731.
- 351 (17) Herlemann DPR, Labrenz M, Jurgens K, Bertilsson S, Waniek JJ, Andersson AF.
352 Transitions in bacterial communities along the 2000 km salinity gradient of the Baltic
353 Sea. *ISME J* 2011; **5**: 1571-1579.
- 354 (18) Holler T, Widdel F, Knittel K, Amann R, Kellermann MY, Hinrichs KU, *et al*. Thermophilic
355 anaerobic oxidation of methane by marine microbial consortia. *ISME J* 2011; **5**: 1946-
356 1956.
- 357 (19) Jørgensen BB, Isaksen MF, Jannasch HW. Bacterial sulfate reduction above 100°C in
358 deep-sea hydrothermal vent sediments. *Science* 1992; **258**: 1756-1757.
- 359 (20) Jørgensen BB, Boetius A. Feast and famine--microbial life in the deep-sea bed. *Nat*
360 *Rev Microbiol* 2007; **5**: 770-781.
- 361 (21) Klindworth A, Pruesse E, Schweer T, Peplies J, Quast C, Horn M, *et al*. Evaluation of
362 general 16S ribosomal RNA gene PCR primers for classical and next-generation
363 sequencing-based diversity studies. *Nucl Acids Res* 2013; **41**: e1.

- 364 (22) Kurr M, Huber R, König H, Jannasch HW, Fricke H, Trincone A, *et al.* *Methanopyrus*
365 *kandleri*, gen. and sp. nov. represents a novel group of hyperthermophilic
366 methanogens, growing at 110°C. *Arch Microbiol* 1991; **156**: 239-247.
- 367 (23) Laso-Pérez R, Wegener G, Knittel K, Widdel F, Harding KJ, Krukenberg V, *et al.*
368 Thermophilic archaea activate butane via alkyl-coenzyme M formation. *Nature* 2016;
369 **539**: 396-401.
- 370 (24) Lever MA, Teske AP. Diversity of methane-cycling Archaea in hydrothermal sediment
371 investigated by general and group-specific PCR primers. *Appl Environ Microbiol*
372 2015; **81**: 1426-1441.
- 373 (25) Lever MA, Torti A, Eickenbusch P, Michaud AB, Santl-Temkiv T, Jørgensen BB. A
374 modular method for the extraction of DNA and RNA, and the separation of DNA pools
375 from diverse environmental sample types. *Front Microbiol* 2015; **6**: 476.
- 376 (26) Lin YS, Koch BP, Feseker T, Ziervogel K, Goldhammer T, Schmidt F, *et al.* Near-
377 surface heating of young rift sediment causes mass production and discharge of
378 reactive dissolved organic matter. *Scient Repts* 2017; **7**: 44864.
- 379 (27) Lizarralde D, Soule SA, Seewald JS, Proskurowski G. Carbon release by off-axis
380 magmatism in a young sedimented spreading centre. *Nature Geosci* 2011; **4**: 50-54.
- 381 (28) Ludwig W, Strunk O, Westram R, Richter L, Meier H, Yadukumar, *et al.* ARB: a
382 software environment for sequence data. *Nucl Acids Res* 2004; **32**: 1363-1371.
- 383 (29) Lundberg DS, Yourstone S, Mieczkowski P, Jones CD, Dangl JL. Practical innovations
384 for high-throughput amplicon sequencing. *Nat Methods* 2013; **10**: 999-1002.
- 385 (30) Martens CS. Generation of short chain organic-acid anions in hydrothermally altered
386 sediments of the Guaymas Basin, Gulf of California. *Appl Geochem* 1990; **5**: 71-76.
- 387 (31) McKay LJ, MacGregor BJ, Biddle JF, Albert DB, Mendlovitz HP, Hoer DR, *et al.* Spatial
388 heterogeneity and underlying geochemistry of phylogenetically diverse orange and
389 white Beggiatoa mats in Guaymas Basin hydrothermal sediments. *Deep Sea*
390 *Research Part I* 2012; **67**: 21-31.
- 391 (32) McKay L, Klokman VW, Mendlovitz HP, LaRowe DE, Hoer DR, Albert D, *et al.* Thermal
392 and geochemical influences on microbial biogeography in the hydrothermal
393 sediments of Guaymas Basin, Gulf of California. *Environ Microbiol Repts* 2016; **8**:
394 150-161.

- 395 (33) McMurdie PJ, Holmes S. Phyloseq: an R package for reproducible interactive analysis
396 and graphics of microbiome census data. *PLoS ONE* 2013; **8**: e61217.
- 397 (34) Meyer S, Wegener G, Lloyd KG, Teske A, Boetius A, Ramette A. Microbial habitat
398 connectivity across spatial scales and hydrothermal temperature gradients at
399 Guaymas Basin. *Front Microbiol* 2013; **4**: 207.
- 400 (35) Nelson DC, Wirsen CO, Jannasch HW. Characterization of large, autotrophic *Beggiatoa*
401 spp. abundant at hydrothermal vents of the Guaymas Basin. *Appl Environ Microbiol*
402 1989; **55**: 2909-2917.
- 403 (36) Ohkuma M, Kudo T. Phylogenetic analysis of the symbiotic intestinal microflora of the
404 termite *Cryptotermes domesticus*. *FEMS Microbiol Lett* 1998; **164**: 389-395.
- 405 (37) Paull CK, Ussler W, Peltzer ET, Brewer PG, Keaten R, Mitts PJ, et al. Authigenic carbon
406 entombed in methane-soaked sediments from the northeastern transform margin of
407 the Guaymas Basin, Gulf of California. *Deep-Sea Res Part II* 2007; **54**: 1240-1267.
- 408 (38) Pearson A, Seewald JS, Eglinton TI. Bacterial incorporation of relict carbon in the
409 hydrothermal environment of Guaymas Basin. *Geochim Cosmochim Acta* 2005; **69**:
410 5477-5486.
- 411 (39) Portail M, Olu K, Dubois SF, Escobar-Briones E, Gelinas Y, Menot L, Sarrazin J.
412 Food-web complexity in Guaymas Basin hydrothermal vents and cold seeps. *PLoS
413 One* 2016; **11**: e0162263.
- 414 (40) Reysenbach AL, Liu YT, Banta AB, Beveridge TJ, Kirshtein JD, Schouten S, et al.
415 (2006). A ubiquitous thermoacidophilic archaeon from deep-sea hydrothermal vents.
416 *Nature* 2006; **442**: 444-447.
- 417 (41) Schutte CA, Teske A, MacGregor BJ, Salman-Carvalho V, Lavik G, Hach P, de Beer
418 D. Filamentous giant *Beggiatoaceae* from the Guaymas Basin are capable of both
419 denitrification and dissimilatory nitrate reduction to ammonium. *Appl Environ
420 Microbiol* 2018; **84**: e02860-17.
- 421 (42) Simoneit BRT, Lonsdale PF. Hydrothermal petroleum in mineralized mounds at the
422 seabed of Guaymas Basin. *Nature* 1982; **295**: 198-202.
- 423 (43) Sørensen KB, Teske A. Stratified communities of active archaea in deep marine
424 subsurface sediments. *Appl Environ Microbiol* 2006; **72**: 4596-4603.

- 425 (44) Teske A, Hinrichs KU, Edgcomb V, Gomez AD, Kysela D, Sylva SP, *et al.* Microbial
426 diversity of hydrothermal sediments in the Guaymas Basin: Evidence for anaerobic
427 methanotrophic communities. *Appl Environ Microbiol* 2002; **68**: 1994-2007.
- 428 (45) Teske A, Edgcomb V, Rivers AR, Thompson JR, Gomez AD, Molyneaux SJ, Wirsén
429 CO. A molecular and physiological survey of a diverse collection of hydrothermal vent
430 *Thermococcus* and *Pyrococcus* isolates. *Extremophiles* 2009; **13**: 905-915.
- 431 (46) Teske A, Callaghan AV, LaRowe DE. Biosphere frontiers of subsurface life in the
432 sedimented hydrothermal system of Guaymas Basin. *Frontiers Microbiol* 2014; **5**:
433 362.
- 434 (47) Teske A, de Beer D, McKay LJ, Tivey MK, Biddle JF, Hoer D, *et al.* The Guaymas Basin
435 hiking guide to hydrothermal mounds, chimneys, and microbial mats: complex
436 seafloor expressions of subsurface hydrothermal circulation. *Frontiers Microbiol*
437 2016; **7**: 75.
- 438 (48) Valentine DL. Adaptations to energy stress dictate the ecology and evolution of the
439 Archaea. *Nature Rev Microbiol* 2007; **5**: 316-323.
- 440 (49) Vigneron A, Cruaud P, Pignet P, Caprais JC, Cambon-Bonavita MA, Godfroy A, Toffin
441 L. Archaeal and anaerobic methane oxidizer communities in the Sonora Margin cold
442 seeps, Guaymas Basin (Gulf of California). *ISME J* 2013; **7**: 1595-1608.
- 443 (50) Wei T, Simko V. R package "corrplot": Visualization of a Correlation Matrix 2017; v.
444 0.84.
- 445 (51) Yu Y, Lee C, Kim J, Hwang S. Group-specific primer and probe sets to detect
446 methanogenic communities using quantitative real-time polymerase chain reaction.
447 *Biotechnol Bioeng* 2005; **89**: 670-679.
- 448